Acta Cryst. (1992). B48, 770–776

Structure of the Quasicrystal-Approximant Phase $Al_{61.3}Cu_{7.4}Fe_{11.1}Cr_{17.2}Si_3$

BY SONG SENG KANG

Laboratoire de Science et Génie des Matériaux Métalliques (CNRS UA159), Ecole des Mines, Parc de Saurupt, F-54042 Nancy CEDEX, France

BERNARD MALAMAN AND GÉRARD VENTURINI

Laboratoire de Chimie du Solide Minéral (CNRS UA158), Université de Nancy I, F-54506 Vandoeuvre les Nancy CEDEX, France

AND JEAN MARIE DUBOIS

Laboratoire de Science et Génie des Matériaux Métalliques (CNRS UA159), Ecole des Mines, Parc de Saurupt, F-54042 Nancy CEDEX, France

(*Received* 27 *September* 1991; *accepted* 7 *May* 1992)

Abstract

The crystal structure of the compound $Al_{61.3}Cu_{7.4}Fe_{11.1}Cr_{17.2}Si_3$ has been determined. The structure is first described by a structure-simulation method and then identified by experimental single-crystal X-ray diffraction. It is a 'one-dimensional approximant' phase. The crystal is orthorhombic (space group *Pnma*) with parameters: $a = 14.582$ (1), $b = 12.321$ (1), $c = 12.363$ (1) Å, $V = 2221$ Å^3, $Z = 1$, $D_x = 4.25$ g cm^{-3}. measurements were performed with Mo $K\alpha$ radiation, $\mu = 98$ cm^{-1}, $F(000) = 2732$, $T = 300$ K, to give $R = 0.038$ ($wR = 0.049$) for 1837 reflections.

1. Introduction

Quasicrystals are materials whose structure cannot be understood within classical crystallography rules. Quasiperiodic structures have long-range orientational order but lack translational periodicity. One typical example is the two-dimensional quasicrystal *e.g.* the decagonal Al–Mn phase (Bendersky, 1985) whose structure is periodic in the third dimension and has orientational symmetry 10/*mmm*. In high-resolution electron microscopy images this phase shows a pattern perpendicular to the tenfold direction which closely resembles Penrose tiling. The Penrose tiling pattern (Penrose, 1974) is constructed from three subtiling units: a convex pentagon, a concave pentagon and a thin rhombus. The convex pentagon is the essential tiling element. During phase transition (decagonal→crystalline), these tiling elements rearrange themselves to form a periodic network of approximant phases. These periodic networks have a well defined pattern with a limited number of subtiling units. Quite often one pattern may correspond to several crystalline phases of different compositions (Dong, Dubois, Kang & Audier, 1992). Their formation is of great importance in the study of phase stability and in structure construction of quasicrystalline phases. They have been related to the rational projection or cut from a higher-dimensional cubic structure (Duneau & Katz, 1985; Elser & Henley, 1985) whereas the irrational projection or cut generates the aperiodic structure. For example, the one-dimensional approximant or quasiperiodic sequence is generated by a one-dimensional cut of irrational slope through a two-dimensional hypercubic lattice. In the quasicrystal case, the sequence is infinite and is a one-dimensional analog of Penrose tiling. Conversely, in the approximant case, the sequence is basically related to the rational slope of the cut or projection. As a matter of fact, each unit segment is actually a fragment of the Fibonacci aperiodic sequence which consists of two intervals, one long (L) and the other short (S) and having a length ratio equal to τ, where τ is the golden mean.

The purpose of this paper is firstly to indicate a method of structure determination which seems likely to be successful for approximant structures, and secondly to illustrate the application of this method to the determination of the structure of a new intermetallic compound having the formula $(AlM)_3M$ where M stands for the transition metals Cu, Fe or Cr.

2. Experimental background

An alloy of nominal composition $Al_{68}Cu_8Fe_{12}Cr_{12}$ was prepared in an induction furnace under a helium atmosphere. In a sample remelted and cooled at

0108-7681/92/060770-07$06.00

5 K min^{-1} to room temperature under an argon atmosphere, two phases have been discovered by means of transmission electron microscopy (Jeol 200CX) observations. One is a monoclinic phase (not discussed in this paper) and the other is an orthorhombic phase (hereafter, the Σ-phase). Fig. 1 shows a series of selected-area electron diffraction (SAED) patterns and Kikuchi line patterns of the Σ-phase taken at different angles. This orthorhombic phase has a primitive structure isotypic with Al_3Mn. Note that the atomic structure of Al_3Mn (Taylor, 1960) has not yet been determined although the space group is known to be *Pnma*. However, its structural relationship to the decagonal phase has been studied in detail by many authors (Fitz Gerald, Withers & Stewart, 1988; Daulton, Kelton & Gibbons, 1991) by means of electron diffraction techniques.

The Σ-phase is an approximant phase. Most of the approximant phases of the decagonal phase are constructed with the same subtiling elements (Dong *et al.*, 1992; Kang & Dubois, 1991). The atomic structure of the Σ-phase may therefore be inferred from an appropriately chosen approximant structure of similar composition. For comparison, the inferred structure is then identified experimentally by means of conventional X-ray techniques on a single crystal. A nearly spherical monocrystalline splinter (diameter $\simeq 60$ μm) was extracted directly from decaprismatic shaped crystals grown inside shrinkage cavities formed in the interior of an ingot. Mircoprobe analysis showed that these crystals contain about 3% silicon yielding a real composition $Al_{61.3}Cu_{7.4}Fe_{11.1}Cr_{17.2}Si_3$. This small amount of silicon results from the impurity of the commercially available elements (*i.e.* Al) which is preferentially concentrated in the Σ-phase.

Preliminary studies were performed with a Weissenberg camera (Cu $K\alpha$). An orthorhombic unit cell was found with the following conditions limiting possible reflections: $0kl$ with $k + l = 2n$ and $hk0$ with $h = 2n$. This leads to two possible space groups: *Pnma* or $Pn2_1a$. The accurate cell parameters, $a = 14.582$ (1), $b = 12.321$ (1) and $c = 12.363$ (1) Å, were determined by least-squares refinement of the 2θ values of 25 independent reflections and antireflections measured on an automatic diffractometer.

3. Structure simulation

Generally, one approximant phase may consist of two one-dimensional periodic sequences oriented according to the condition $n\pi/10$ (where n is an

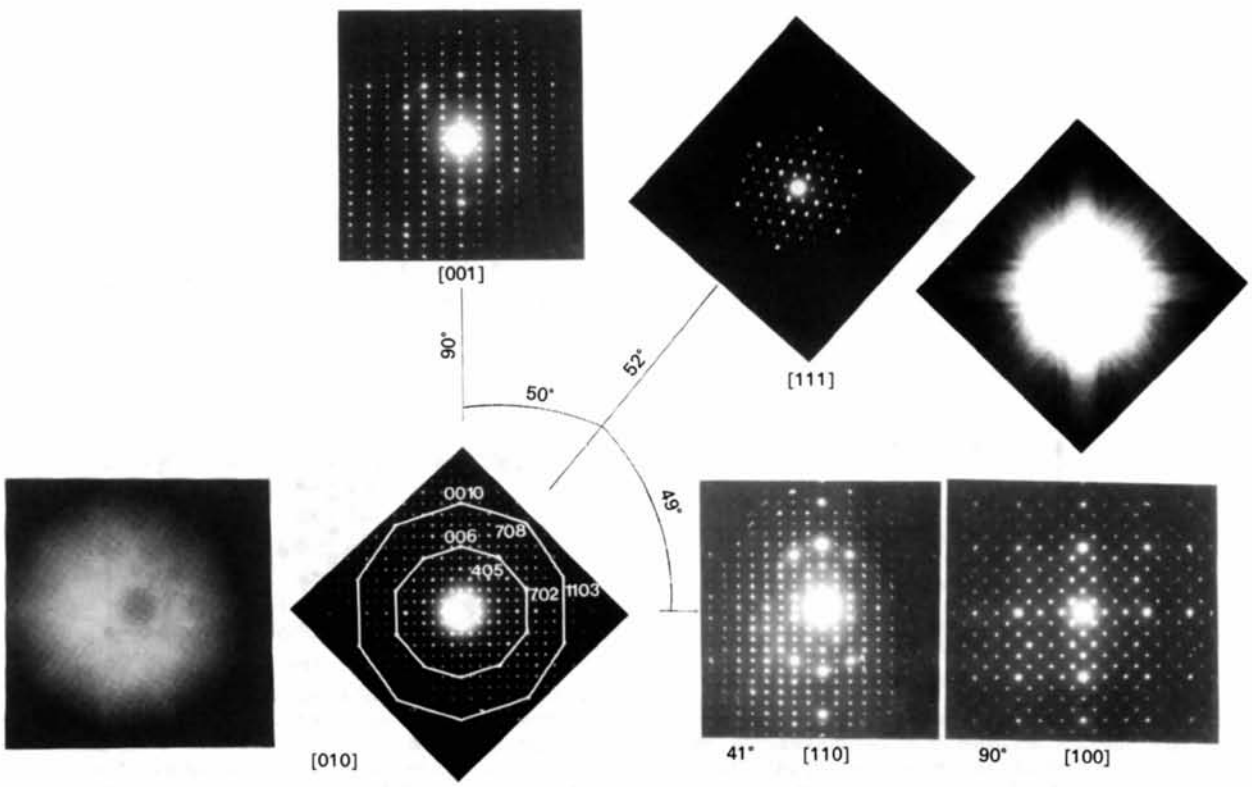

Fig. 1. Stereo representation of typical electron diffraction patterns of the orthorhombic phase $(AlM)_3M$. Two Kikuchi line patterns are also given for the pseudo-tenfold direction and the pseudo-fourfold direction.

integer) perpendicular to the pseudo-tenfold axis (Kang & Dubois, 1991). However, this is not the case for the Σ-phase. The Σ-phase has only one approximant sequence along the pseudo-tenfold direction and is therefore referred to as a 'one-dimensional approximant' phase. This point is illustrated by the SAED pattern along the [010] axis (Fig. 1), where the intense spots are oriented almost symmetrically at an angle of 36°. They can be connected to form a decagon and two decagons are laid out in the pattern. If the approximant sequence exists, the intense spots in both decagons must lie in the same direction due to the ordered arrangement of the subtiling elements under the condition $n\pi/10$. Nevertheless, there are only (006) and (0010) intense spots lying in the same direction [001]. The segment of the sequence is thus the distance $c \simeq 12.4$ Å $= \tau^2 d_0$, where $d_0 = L \simeq 4.7$ Å is the edge length of the subtiling elements. Referring to Kang & Dubois (1991), $\tau^2 d_0$ corresponds to the *LSL* sequence. The simplest tiling for this sequence is an analogous linking of two pentagons (Fig. 2*a*).

The two-dimensional structure construction of the approximant phases needs two one-dimensional periodic sequences. For instance, we may not be able to generate the Σ-phase pattern since we have only one approximant sequence. However, if we place the chain of pentagons in the Σ-phase unit cell as shown in Fig. 2(*a*), we may deduce its sublattice under the symmetry operation of *Pnma* (Fig. 2*b*). The questions now are, how can the three-dimensional network be simulated and where are the atoms inside this three-dimensional network.

Among the results reported so far for the approximant phases, the orthorhombic $Al_{60}Mn_{11}Ni_4$ (hereafter the φ-phase) of space group *Bbmm* (Robinson, 1954) is the most suitable structure to use to simulate the atomic configuration of the Σ-phase (Fig. 3). Firstly, both structures are centrosymmetric with almost equal *b* lattice parameters, 12.5 Å for the φ-phase and 12.4 Å for the Σ-phase. Secondly, they are both packed according to the pentagon and thin subunits in a two-dimensional pattern (compare Figs. 2*b* and 3*a*). The φ-phase consists of two types of layers, the flat layer *A* and the corrugated layer *B* stacked perpendicular to the *b* axis. The two-dimensional subunits can thus be further described in terms of three-dimensional polyhedral units as shown in Fig. 3(*b*).

From the above argument, we assume here that the three-dimensional units can also form the

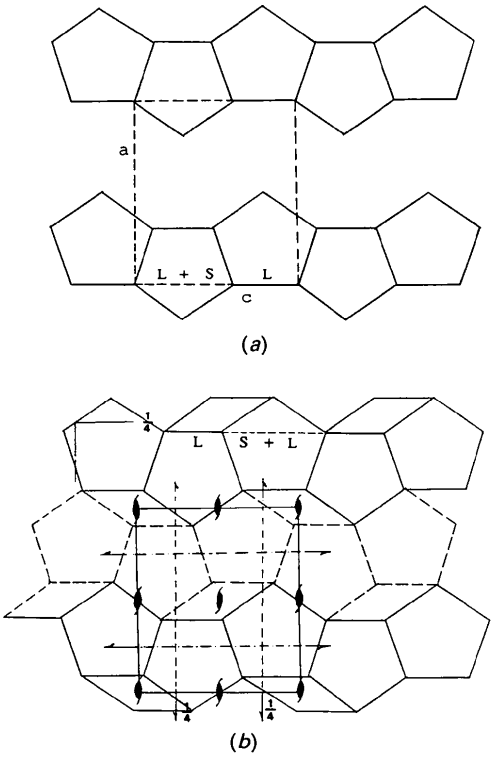

Fig. 2. Two-dimensional structure simulation. (*a*) Two chains of pentagon subunits simulated from one-dimensional approximant sequence *LSL* and (*b*) application on pattern (*a*) of the symmetry operations of space group *Pnma* and resulting two-dimensional sublattice of $(AlM)_3M$ seen along the pseudo-tenfold direction.

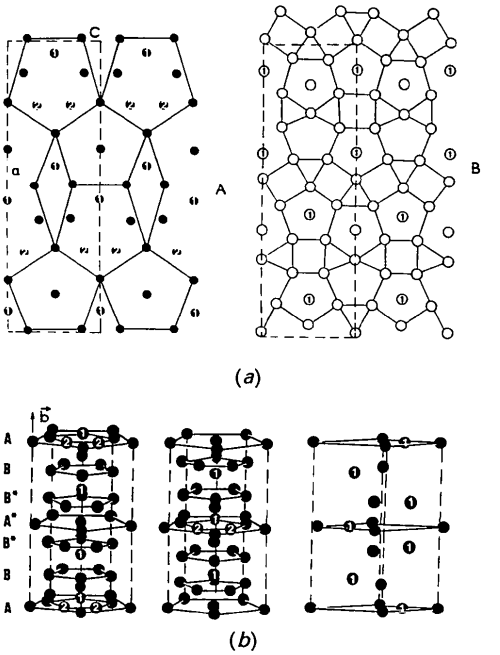

Fig. 3. Crystal structure of *B*-centred orthorhombic $Al_{60}Mn_{11}Ni_4$. (*a*) Projection views of the flat layer *A* at $y = 0.25$ and of the corrugated layer *B* at $y \simeq 0.1$ and 0.4. (*b*) Three-dimensional subunits stacked by the *A*- and *B*-type layers. *A** and *B** are two layers generated by a twofold symmetry operation applied to *A* and *B* layers, respectively. Dots (1) denote Mn atoms and dots (2) denote Ni atoms, the balance being Al atoms.

Σ-phase cell and we pack these three-dimensional units according to the two-dimensional sublattice pattern. Surprisingly, all the atoms agree well with the symmetry operation of space group *Pnma*. Of course, small adjustments to the atomic positions are still necessary due to the changes of composition and cell parameters. If the lattice nodes have not yet been determined, the elemental distribution is still obscure except for those Al atoms that obviously occupy the *A* layer. Table 1 presents a list of atomic parameters calculated from the simulated structure. Computation of the powder X-ray diffraction pattern as well as single-crystal data immediately leads to satisfactory agreement with the experimental data (see next section). The Σ-phase also consists of two layers, its atomic configuration can be seen in Fig. 4. Note that, anticipating the next section, the atomic positions are close to the measured parameters (Table 2).

Table 1. *Atomic positions obtained from the simulated structure*

M denotes the transition metals Fe, Cr or Cu.

		x	*y*	*z*
1	Al	0.3981	0.2500	0.4839
2	Al	0.3981	0.2500	0.8856
3	Al	0.1132	0.2500	0.9460
4	Al	0.1867	0.2500	0.6643
5	Al	0.1030	0.2500	0.3840
6	Al	0.1510	0.2500	0.1610
7	Al	0.4530	0.2500	0.2737
8	*M*	0.2745	0.2500	0.0008
9	*M*	0.4290	0.2500	0.0644
10	*M*	0.2814	0.2500	0.3301
11	*M*	0.4544	0.2500	0.6844
12	Al	0.3171	0.3530	0.1539
13	Al	0.8693	0.4380	0.5290
14	Al	0.1853	0.4350	0.2923
15	Al	0.3569	0.4050	0.6683
16	Al	0.2416	0.3924	0.8014
17	Al	0.0528	0.4050	0.7770
18	Al	0.0388	0.3996	0.5475
19	Al	0.2388	0.3924	0.4831
20	*M*	0.5491	0.4320	0.3140
21	Al	0.4942	0.4350	0.1566
22	Al	0.1820	0.4350	0.0386
23	Al	0.3768	0.4350	0.3599
24	Al	0.4990	0.6080	0.4767
25	*M*	0.3191	0.5550	0.1787

4. Single-crystal X-ray diffraction

Structure refinement

Data collection was performed on an Enraf–Nonius CAD-4 automatic diffractometer. A total of 3401 reflections ($1 \le \theta \le 30°$, $h_{max} = 21$, $k_{max} = 18$, $l_{max} = 18$) were measured in θ–2θ mode using graphite-monochromated Mo $K\alpha$ radiation. Intensity variations of the (702), (0010) and (523) standard reflections were less than 0.3%. Owing to the small size of the crystal, only 1837 reflections with $\sigma(I)/I < 0.30$ were retained for refinement of the 214 variable parameters (Table 2). Absorption was neglected ($\mu = 98\ cm^{-1}$, *i.e.* $\mu r < 0.30$). Atomic scattering factors for neutral atoms and anomalous-dispersion corrections were taken from *International Tables for X-ray Crystallography* (1974, Vol. IV). All computer programs used here were from Sheldrick (1976).*

Using atomic positions deduced from the simulated model as a starting point, preliminary refinement in the space group *Pnma* leads to a reliability factor $R = 0.29$ (considering an average value for *M* atoms $= f_{Cr}$). This result confirms the assumptions made for the simulated structure.†

The elemental distribution must be improved, however, since the real composition ($Al_{61.4}M_{35.7}Si_{2.9}$)

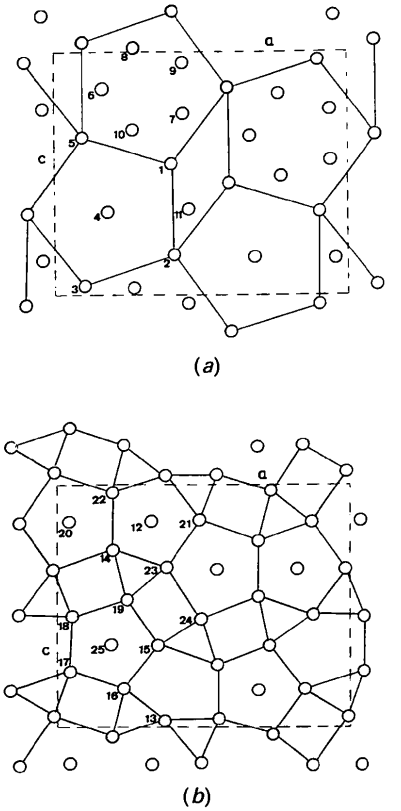

Fig. 4. Crystal structure of $Al_{61.3}Cu_{7.4}Fe_{11.1}Cr_{17.2}Si_3$ showing the projection patterns for (*a*) the flat layer *A* at $y = 0.25$ and (*b*) the corrugated layer *B* at $y \simeq 0.1$ and 0.4.

* A list of structure factors has been deposited with the British Library Document Supply Centre as Supplementary Publication No. SUP 55273 (13 pp.). Copies may be obtained through The Technical Editor, International Union of Crystallography, 5 Abbey Square, Chester CH1 2HU, England. [CIF reference: CR0395]

† An attempt was made to solve the structure using direct methods (Sheldrick, 1985) but none of the attempted refinements led to a residual better than $R = 0.35$. Nevertheless, it is worth noting that the normalized structure-factor distribution $E(H)$ is hypercentrosymmetric.

Table 2. *Atomic positions, occupancy factors m_j and individual anisotropic thermal U_{ij} parameters (Å^2) obtained from the single-crystal X-ray study*

The estimated standard deviations are given in parentheses. x, $\frac{1}{4}$, z: position 4(*c*), point symmetry *m*. x, y, z: position 8(*d*), point symmetry 1. $T_j = \exp[-2\pi^2(U_{11}h^2a^{*2} + U_{22}k^2b^{*2} + U_{33}l^2c^{*2} + 2U_{12}hka^*b^* + 2U_{13}hla^*c^* + 2U_{23}klb^*c^*)]$.

	x	y	z	m_j	U_{11}	U_{22}	U_{33}	U_{12}	U_{13}	U_{23}
AA(1)	0.4004 (5)	0.2500 (0)	0.4610 (6)	0.50 (0)	0.004 (3)	0.034 (5)	0.004 (3)	0.000 (0)	−0.002 (2)	0.000 (0)
AA(2)	0.4059 (4)	0.2500 (0)	0.8383 (6)	0.50 (0)	0.002 (2)	0.015 (3)	0.001 (3)	0.000 (0)	0.001 (2)	0.000 (0)
AA(3)	0.0984 (5)	0.2500 (0)	0.9606 (6)	0.50 (0)	0.005 (3)	0.037 (5)	0.005 (3)	0.000 (0)	−0.003 (2)	0.000 (0)
AA(4)	0.1814 (5)	0.2500 (0)	0.6572 (7)	0.50 (0)	0.014 (3)	0.006 (2)	0.009 (3)	0.000 (0)	−0.003 (3)	0.000 (0)
AA(5)	0.0959 (4)	0.2500 (0)	0.3491 (7)	0.50 (0)	0.003 (2)	0.021 (3)	0.007 (3)	0.000 (0)	−0.000 (3)	0.000 (0)
AM(6)	0.1702 (2)	0.2500 (0)	0.1536 (3)	0.51 (1)	0.007 (1)	0.006 (1)	0.004 (1)	0.000 (0)	−0.002 (1)	0.000 (0)
AM(7)	0.4410 (3)	0.2500 (0)	0.2568 (3)	0.54 (1)	0.008 (2)	0.007 (2)	0.006 (2)	0.000 (0)	0.002 (1)	0.000 (0)
AM(8)	0.2750 (2)	0.2500 (0)	0.9831 (3)	0.53 (1)	0.004 (1)	0.005 (1)	0.004 (2)	0.000 (0)	0.000 (1)	0.000 (0)
AM(9)	0.4430 (2)	0.2500 (0)	0.0468 (3)	0.54 (1)	0.004 (1)	0.007 (2)	0.005 (2)	0.000 (0)	−0.001 (1)	0.000 (0)
AM(10)	0.2692 (2)	0.2500 (0)	0.3238 (3)	0.55 (1)	0.006 (1)	0.007 (2)	0.005 (2)	0.000 (0)	−0.001 (1)	0.000 (0)
AM(11)	0.4588 (2)	0.2500 (0)	0.6481 (3)	0.59 (1)	0.004 (1)	0.010 (1)	0.003 (1)	0.000 (0)	0.001 (1)	0.000 (0)
BA(12)	0.3200 (3)	0.3531 (3)	0.1535 (4)	1.24 (3)	0.012 (2)	0.007 (2)	0.012 (2)	0.001 (1)	0.000 (2)	−0.001 (2)
BA(13)	0.8713 (2)	0.4369 (3)	0.5337 (3)	1.28 (3)	0.007 (2)	0.010 (2)	0.012 (2)	0.001 (1)	0.002 (1)	0.002 (2)
BA(14)	0.1881 (2)	0.4341 (3)	0.2708 (3)	1.34 (3)	0.009 (2)	0.009 (2)	0.008 (2)	0.001 (1)	−0.003 (1)	0.002 (1)
BA(15)	0.3434 (3)	0.3801 (4)	0.6604 (5)	1.06 (3)	0.009 (2)	0.019 (2)	0.018 (3)	0.006 (2)	−0.001 (2)	0.001 (2)
BA(16)	0.2272 (3)	0.3790 (4)	0.8395 (4)	1.10 (3)	0.012 (2)	0.015 (2)	0.009 (2)	0.000 (2)	0.000 (2)	0.003 (2)
BA(17)	0.0465 (4)	0.3824 (4)	0.7642 (5)	1.05 (3)	0.012 (3)	0.021 (3)	0.014 (3)	−0.009 (2)	0.004 (2)	0.002 (2)
BA(18)	0.0507 (3)	0.3749 (4)	0.5420 (4)	1.13 (3)	0.009 (2)	0.016 (2)	0.011 (2)	−0.002 (2)	−0.001 (2)	−0.001 (2)
BA(19)	0.2359 (3)	0.3768 (4)	0.4738 (4)	1.08 (3)	0.011 (2)	0.013 (3)	0.007 (2)	0.000 (2)	0.002 (2)	0.002 (2)
BA(20)	0.5415 (2)	0.3901 (4)	0.3483 (4)	1.32 (3)	0.005 (2)	0.033 (2)	0.012 (2)	0.002 (1)	−0.003 (2)	−0.008 (2)
BM(21)	0.4854 (2)	0.4360 (2)	0.1499 (3)	0.85 (2)	0.013 (1)	0.009 (1)	0.008 (1)	0.002 (1)	−0.001 (1)	−0.002 (1)
BM(22)	0.1858 (2)	0.4371 (3)	0.0399 (2)	0.91 (2)	0.009 (1)	0.008 (1)	0.009 (1)	−0.002 (1)	0.003 (1)	−0.001 (1)
BM(23)	0.3703 (2)	0.4363 (2)	0.3403 (2)	0.93 (2)	0.005 (1)	0.008 (1)	0.012 (1)	0.000 (1)	0.001 (1)	0.003 (1)
BM(24)	0.5164 (3)	0.5774 (2)	0.4541 (3)	0.91 (2)	0.044 (2)	0.005 (1)	0.011 (1)	−0.002 (1)	0.013 (1)	0.003 (1)
BM(25)	0.3192 (1)	0.5533 (2)	0.1535 (2)	1.12 (2)	0.006 (1)	0.009 (1)	0.004 (1)	0.000 (1)	0.001 (1)	−0.000 (1)

Table 3. *Some interatomic distances ($d < 3$ Å) as calculated from the single-crystal data only for sites* 11, 12, 15 *and* 24

The estimated standard deviations are given in parentheses.

	Neighbour	Distance (Å)		Neighbour	Distance (Å)
AM(11)	2*BA*(15)	2.329 (6)	*BA*(15)	*AM*(11)	2.329 (6)
	2*BA*(17)	2.340 (6)		*BM*(25)	2.510 (6)
	AA(3)	2.439 (8)		*BM*(24)	2.542 (6)
	AA(1)	2.465 (8)		*BA*(14)	2.705 (6)
	AA(2)	2.475 (7)		*BM*(22)	2.734 (6)
	2*BM*(24)	2.500 (4)		*BA*(16)	2.789 (7)
BA(12)	*BM*(25)	2.467 (4)		*BA*(19)	2.790 (7)
	AM(7)	2.521 (5)		*AA*(4)	2.856 (8)
	AM(6)	2.526 (4)		*AA*(2)	2.870 (8)
	BA(12)	2.540 (7)	*BM*(24)	*BM*(24)	2.270 (6)
	AM(8)	2.546 (5)		*AM*(11)	2.500 (4)
	AM(9)	2.563 (5)		*BA*(15)	2.542 (6)
	AM(10)	2.568 (5)		*BA*(17)	2.569 (6)
	BA(14)	2.607 (5)		*BA*(20)	2.614 (6)
	BM(21)	2.608 (5)		*AA*(1)	2.663 (6)
	BM(22)	2.621 (5)		*BA*(20)	2.678 (6)
	BM(23)	2.631 (5)		*AA*(3)	2.707 (6)
	BA(13)	2.643 (6)			

measured by the microprobe does not agree with the simulated one (*i.e.* $Al_{79.5}M_{20.5}$). Further refinements of the occupancy factors m_j show that the chemical distribution is very complicated in this structure. From the difference between refined site-occupancy parameter values (Table 2) and theoretical values, four types of site can be distinguished: *AA*(1) to *AA*(5), sites fully occupied by Al atoms in *A*-type layers; *AM*(6) to *AM*(11), sites mainly occupied by transition-metal atoms in *A*-type layers; *BA*(12) to *BA*(20), sites mainly occupied by Al atoms in *B*-type layers; *BM*(21) to *BM*(25), sites mainly occupied by transition-metal atoms in *B*-type layers.

Note that the first *A* or *B* in the notation denotes *A*-type layers at $y = \frac{1}{4}$ and $\frac{3}{4}$ or *B*-type layers at $y \simeq 0.4$ and 0.6, respectively. The following *A*(*i*) or *M*(*i*) denote the nature of the atoms, *A* for aluminium and *M* for transition metals (Cu, Fe or Cr) lying at site *i*. With these atomic distributions, the corresponding reliability factor R is 0.095. This reduces to a final value of $R = 0.038$ $\{wR = 0.049$ with the weighting scheme $w = [\sigma^2(F) + 0.010155F^2]^{-1}$; $\Delta\rho_{max} = 1.09$ e Å^{-3} and $\Delta\rho_{min} = -1.2$ e Å$^{-3}\}$ when the refinement is carried out using individual and anisotropic thermal parameters U_{ij} and free occupancy factors m_j for all atoms except *AA*(1)–*AA*(5). Atomic parameters as well as U_{ij} values and occupancy factors are given in Table 2. Some interatomic distances are listed in Table 3 and the structure is drawn in Fig. 4.

Chemical distribution

Electron density syntheses (see occupancy factors in Table 2 for comparison) suggest that only atoms *AA*(1–5) which form the sublattice [excluding site *AA*(4), see Fig. 4*a*] of layer *A* are fully occupied by Al atoms. The rest of the atoms (6–25), however, are disordered in the structure.

To tackle the problem of the measured composition with respect to m_j values and interatomic dis-

tances, we here propose a somewhat more suitable atomic distribution for the Σ-phase structure. Some examples are given below in order to explain how the distribution is selected.

The occupancy factor $m_j = 0.59$ observed for site $AM(11)$ indicates that it is preferentially occupied by a Cu atom since the Cu atom has the highest electron density here. However, if the site is totally occupied by Cu atoms with $m_j = 0.524$, it still deviates from the theoretical value ($m_j = 0.5$). The best compromise is obtained by substitution of $\frac{1}{4}$ Cr atoms and $\frac{3}{4}$ Cu atoms. This gives a value of m_j equal to the theoretical value.

By contrast, the m_j value of 0.91 for the site $BM(24)$ indicates that Cr atoms are good candidates to occupy the site but they must share it with other atoms which have lower electron density. In this case, we look for Al- and Si-atom substitution since the interatomic distance must also be considered. The Al atom has a larger radius and is therefore too big for substitution. Note that the distance $BM(24)$—$BM(24)$ is 2.270 Å, whereas, the shortest Al—Al = $BA(12)$—$BA(12)$ distance is 2.540 Å (Table 3). Thus, only Si atoms are suitable. Substituting $\frac{1}{4}$ Si atoms for each $BM(24)$ atom gives an occupancy equal to a more acceptable value of 1.037. Note that the $BM(24)$ atom is situated inside a rhombohedral three-dimensional unit and surrounded by pentagonal three-dimensional units. The presence of Si atoms in this position is not at all by accident. Since their substitution at the site is compulsory for such a configuration, this explains why the Σ-phase structure is stabilized by Si atoms.

This leads to a new elemental distribution which can be described in terms of two separate unit cells, namely cell (1) and cell (2). The average structure then contains $\frac{3}{4}$ cell (1) and $\frac{1}{4}$ cell (2) (Table 4). Cell (1) consists mainly of Al atoms in layer B, and is expanded along the b axis. However, this expansion is compensated for by cell (2) which consists principally of small atoms (Cr, Fe, Si and Cu). This model tends to the composition $Al_{59}Cu_{8.9}Fe_{11.8}Cr_{17.7}Si_{2.6}$ which is close to the measured value (see §2). Most of the multiplicity parameters are in good agreement with the ideal values.

Table 4. *Corrected occupancy factors m_j (see text)*

	$\frac{3}{4}$ Cell (1) + $\frac{1}{4}$ Cell (2)	m_j
$AA(1)$	$\frac{3}{4}$Al + $\frac{1}{4}$Al	0.500
$AA(2)$	$\frac{3}{4}$Al + $\frac{1}{4}$Al	0.500
$AA(3)$	$\frac{3}{4}$Al + $\frac{1}{4}$Al	0.500
$AA(4)$	$\frac{3}{4}$Al + $\frac{1}{4}$Al	0.500
$AA(5)$	$\frac{3}{4}$Al + $\frac{1}{4}$Al	0.500
$AM(6)$	$\frac{3}{4}$Cr + $\frac{1}{4}$Fe	0.504
$AM(7)$	$\frac{3}{4}$Fe + $\frac{1}{4}$Cr	0.499
$AM(8)$	$\frac{3}{4}$Cr + $\frac{1}{4}$Cu	0.496
$AM(9)$	$\frac{3}{4}$Fe + $\frac{1}{4}$Cr	0.500
$AM(10)$	$\frac{3}{4}$Fe + $\frac{1}{4}$Fe	0.498
$AM(11)$	$\frac{3}{4}$Cu + $\frac{1}{4}$Cr	0.501
$BA(12)$	$\frac{3}{4}$Al + $\frac{1}{4}$Cr	1.021
$BA(13)$	$\frac{3}{4}$Al + $\frac{1}{4}$(Cu + Cr)	1.014
$BA(14)$	$\frac{3}{4}$Al + $\frac{1}{4}$Cu	1.028
$BA(15)$	$\frac{3}{4}$Al + $\frac{1}{4}$Al	1.058
$BA(16)$	$\frac{3}{4}$Al + $\frac{1}{4}$Al	1.101
$BA(17)$	$\frac{3}{4}$Al + $\frac{1}{4}$Al	1.043
$BA(18)$	$\frac{3}{4}$Al + $\frac{1}{4}$Si	1.104
$BA(19)$	$\frac{3}{4}$Al + $\frac{1}{4}$Al	1.083
$BA(20)$	$\frac{3}{4}$Al + $\frac{1}{4}$Cu	1.037
$BM(21)$	$\frac{1}{4}$(2Al + 1Cu) + $\frac{1}{4}$Cr	1.028
$BM(22)$	$\frac{3}{4}$Cr + $\frac{1}{4}$Al	1.025
$BM(23)$	$\frac{3}{4}$(Al + Cu) + $\frac{1}{4}$Cr	1.034
$BM(24)$	$\frac{3}{4}$Cr + $\frac{1}{4}$Si	1.015
$BM(25)$	$\frac{3}{4}$Fe + $\frac{1}{4}$Fe	1.004

U_{ij} parameters

The structure proposed above also explains why some atomic thermal vibrations are strongly anisotropic along the b axis (Table 2). In fact, in such a structure, the U_{ij} parameters describe more than thermal motions, and therefore it is better to consider them as mean-square atomic displacement parameters. For example, the values are very important in the b direction (U_{22}) but are small in the a (U_{11}) and c (U_{33}) directions for Al-atom sites in the A-layer sublattice. This is due to the slight change in the constant b in the two distinct unit cells. Since most of the atoms are disordered, when a large atom is replaced by a small one, the neighbouring atoms will shift slightly so as to fill the voids resulting from the different atomic radii, and *vice versa* for the small atoms when these are replaced by the big atoms. As a result, each atom shows a larger limit of local displacement in one or more directions (see values underlined in Table 2).

Interatomic distances

Some interatomic distances are very short for the average Σ-phase structure. In this section, we consider three examples of Al–Al, Al–M and M–M pairs and discuss the short distances found in both the Σ-phase and some other crystalline phases (Table 5).

In the Al_6Mn structure, the shortest distance between two Al atoms is 2.57 Å. According to Nicol (1953), this is probably due to electron transfer from Al atoms to neighbouring Mn atoms. If this is so, the short $BA(12)$—$BA(12)$ distance of 2.540 Å may be due to electron transfer from Al atoms to the nearest transition metals. Nevertheless, similar distances have also been obtained in other phases such as θ-Al_7Cr (Cooper, 1960).

For the short distance Al—M *i.e.* $BA(15)$—$AM(11)$, as revealed by the U_{ij} parameters of related atoms, a more acceptable value can be obtained. Without resulting in any other interatomic distance shorter than the minimal Al—M = 2.445 Å (Walford, 1965) and Al—Al = 2.559 Å (Cooper, 1960), the atom $BA(15)$ is allowed to be displaced by

Table 5. *Shortest interatomic distance in the Σ-$(AlM)_3M$ phase and comparable distances found in other crystalline phases*

	Type of neighbour	Shortest interatomic distance (Å) in Σ-phase	Comparable interatomic distance (Å)
BA(12)	*BA*(12)	2.541 (7)	2.559 in θ-Al_7Cr (Cooper, 1960)
BA(15)	*AM*(11)	2.329 (6)	2.445 in Al_6Fe (Walford, 1965)
			2.460 in α-$Al_{13}Cr_4Si_4$ (Robinson, 1953)
			2.511 in Al_7Cu_2Fe (Brown & Brown, 1956)
BM(24)	*BM*(24)	2.270 (6)	2.253 in σ-Fe-Cr (Bergman & Shoemaker, 1954)
			2.400 in α-$(AlCu)_6(FeCu)$ (Walford, 1965)

$\Delta x = 0$, $\Delta y = 0.014$ and $\Delta z = -0.012$. The *BA*(15)—*AM*(11) distance so obtained is about 2.445 Å, which is equivalent to the shortest values observed in Al_6Fe.

In the last example, the short distance *BM*(24)—*BM*(24) is 2.270 Å with a standard deviation of 0.006 (Table 3). Some equivalent interatomic distances have been reported by Bergman & Shoemaker (1954) in the σ-Fe-Cr phase. In this σ-phase, the shortest distance (2.253 Å) is smaller than for *BM*(24)—*BM*(24). Thus, the short distance obtained here between two transition-metal atoms is quite acceptable.

In fact, the short interatomic distances observed in the Σ-phase structure are linked to the directions and values of the mean-square displacements (U_{ij}) of the corresponding atoms, *i.e.* *AM*(11), *BA*(15) and *BM*(24) (Table 2). Most of the mean-square-displacement ellipsoids of the atoms are nearly spherical except for the three atoms quoted previously and the four atoms forming the sublattice in the layer *A*, *i.e.* *AA*(1)—*AA*(3), *AA*(5) and *BA*(20).

5. Concluding remarks

The orthorhombic phase $(AlM)_3M$ is a 'one-dimensional approximant' phase. This phase can be determined by a simulation method starting from a known structure $Al_{60}Mn_{11}Ni_4$. Its structure consists of stacks of two distinct layers, one flat and one corrugated along the [010] direction. The characteristic pattern obtained is that of the sublattice packed with two subunits: pentagon and thin rhombus in the flat layer. The simulated structure has been verified by experimental X-ray diffraction on a single crystal. The simulated atom positions show good agreement with the measured ones but a complete determination of the chemical distribution was unsuccessful due to the disordered agreement which exists in the crystal. This disordered system shows that the Al atoms can be interchanged with transition-metal atoms in most of the sites except for sites at the vertex and the centre of the pentagon subunit in the flat layer. Since this structure is closely related to the decagonal phase, the chemical distribution in this quasicrystalline phase may also be somewhat disordered. This structure is stabilized by the presence of Si atoms lying within two pentagon subunits.

References

BENDERSKY, L. (1985). *Phys. Rev. Lett.* **55**, 1461–1463.

BERGMAN, G. & SHOEMAKER, D. P. (1954). *Acta Cryst.* **7**, 857–865.

BROWN, M. G. & BROWN, P. J. (1956). *Acta Cryst.* **9**, 911–914.

COOPER, M. J. (1960). *Acta Cryst.* **13**, 257–263.

DAULTON, T. L., KELTON, K. F. & GIBBONS, P. C. (1991). *Philos. Mag. B*, **63**, 687–714.

DONG, C., DUBOIS, J. M., KANG, S. S. & AUDIER, M. (1992). *Philos. Mag. B*, **65**, 107–126.

DUNEAU, M. & KATZ, A. (1985). *Phys. Rev. Lett.* **54**, 2688–2691.

ELSER, V. & HENLEY, C. L. (1985). *Phys. Rev. Lett.* **55**, 2883–2886.

FITZ GERALD, J. D., WITHERS, R. L. & STEWART, A. M. (1988). *Philos. Mag. B*, **58**, 15–33.

KANG, S. S. & DUBOIS, J. M. (1991). *International Conference on Polytypes, Modulated Structures and Quasicrystals, 'Mospoq'* 91. Balatonszéplak, Hungary. To appear in *Phase Transitions*.

NICOL, A. D. I. (1953). *Acta Cryst.* **6**, 285–293.

PENROSE, R. (1974). *Bull. Inst. Math. Appl.* **10**, 266–271.

ROBINSON, K. (1953). *Acta Cryst.* **6**, 854–859.

ROBINSON, K. (1954). *Acta Cryst.* **7**, 494–497.

SHELDRICK, G. M. (1976). *SHELX*76. Program for crystal structure determination. Univ. of Cambridge, England.

SHELDRICK, G. M. (1985). *Crystallographic Computing* 3, edited by G. M. SHELDRICK, C. KRÜGER & R. GODDARD, pp. 175–189. Oxford Univ. Press.

TAYLOR, M. A. (1960). *Acta Metall.* **8**, 256–262.

WALFORD, L. K. (1965). *Acta Cryst.* **18**, 287–291.